PLUME OBSERVABLES AND COUNTERMEASURES

Frederick P. Boynton

Physical Dynamics, Incorporated

Prepared for:

Air Force Cambridge Research Laboratories

31 July 1972

AFCRL-72-0632 PD-72-027

PLUME OBSERVABLES AND COUNTERMEASURES

by

Frederick P. Boynton

PHYSICAL DYNAMICS, INC.
P.O. Box 604
College Park Station
Detroit, Michigan 48221

Contract No. F19628-72-C-0006
Project No. 8692

SEMI-ANNUAL TECHNICAL REPORT NO. 2

31 July 1972

Contract Monitor: Alva T. Stair
Optical Physics Laboratory

Approved for public release; distribution unlimited

Sponsored by
Defense Advanced Research Projects Agency
ARPA Order No. 1856

Monitored by
AIR FORCE CAMBRIDGE RESEARCH LABORATORIES
AIR FORCE SYSTEMS COMMAND
UNITED STATES AIR FORCE
BEDFORD, MASSACHUSETTS 01730

UNCLASSIFIED
Security Classification

DOCUMENT CONTROL DATA - R & D
(Security classification of title, body of abstract and indexing annotation must be entered when the overall report is classified)

1. ORIGINATING ACTIVITY (Corporate author)
Physical Dynamics, Inc.
P.O. Box 1069
Berkeley, Calif. 94701

2a. REPORT SECURITY CLASSIFICATION
UNCLASSIFIED

2b. GROUP

3. REPORT TITLE
PLUME OBSERVABLES AND COUNTERMEASURES

4. DESCRIPTIVE NOTES (Type of report and inclusive dates)
Scientific. Interim.

5. AUTHOR(S) (First name, middle initial, last name)
Frederick P. Boynton

6. REPORT DATE
31 July 1972

7a. TOTAL NO. OF PAGES
~~62~~ 66

7b. NO. OF REFS
17

8a. CONTRACT OR GRANT NO. F19628-72-C-0006
ARPA Order No. 1856

b. PROJECT, Task, Work Unit No.
8692 n/a n/a

c. DoD Element 62301D

d. DoD Subelement n/a

9a. ORIGINATOR'S REPORT NUMBER(S)
PD-72-027
Semi-Annual Technical Report No. 2

9b. OTHER REPORT NO(S) (Any other numbers that may be assigned this report)
AFCRL-72-0632

10. DISTRIBUTION STATEMENT
A - Approved for public release; distribution unlimited.

11. SUPPLEMENTARY NOTES
This research was supported by the Defense Advanced Research Projects Agency.

12. SPONSORING MILITARY ACTIVITY
Air Force Cambridge Research Laboratories (OP)
L.G. Hanscom Field
Bedford, Massachusetts 01730

13. ABSTRACT

Further work on the radiative behavior of rocket exhaust plumes at high altitude is reported. Comparisons of calculated flow fields with wind-tunnel test data indicate that agreement is generally satisfactory if allowances are made for absolute calibrations of the data. Calculations of a plume emission according to some proposed mechanisms have been performed. It appears that production of OH by O atom attack on secondary H atoms in hydrocarbon fragments can result in substantial chemiluminescent emission from H_2O formed by subsequent reaction of the OH. Some semi-quantitative analogies between rocket exhaust flows and material releases in the upper atmosphere are discussed, and derivations directed toward comparing collision energy distributions at very high altitudes are presented.

DD FORM 1 NOV 68 1473

UNCLASSIFIED
Security Classification

14.

KEY WORDS	LINK A		LINK B		LINK C	
	ROLE	WT	ROLE	WT	ROLE	WT
Exhaust Plume Observables						

AFCRL-72-0632 PD-72-027

PLUME OBSERVABLES AND COUNTERMEASURES

by

Frederick P. Boynton

PHYSICAL DYNAMICS, INC.
P.O. Box 604
College Park Station
Detroit, Michigan 48221

Contract No. F19628-72-C-0006
Project No. 8692

SEMI-ANNUAL TECHNICAL REPORT NO. 2

31 July 1972

Contract Monitor: Alva T. Stair
Optical Physics Laboratory

Sponsored by
Defense Advanced Research Projects Agency
ARPA Order No. 1856

Monitored by
AIR FORCE CAMBRIDGE RESEARCH LABORATORIES
AIR FORCE SYSTEMS COMMAND
UNITED STATES AIR FORCE
BEDFORD, MASSACHUSETTS 01730

i b

ARPA Order No. 1856

Program Code No. 1E40

Contractor: Physical Dynamics, Inc.

Effective Date of Contract: 1 July 1971

Contract No. F19628-72-C-0006

Principal Investigator and Phone No.
Mr. Frederick P. Boynton/(415)-848-3063

AFRCL Project Scientist and Phone No.
Dr. Alva T. Stair/(617)-861-4911

Contract Expiration Date: 31 December 1973

ABSTRACT

Further work on the radiative behavior of rocket exhaust plumes at high altitude is reported. Comparisons of calculated flow fields with wind-tunnel test data indicate that agreement is generally satisfactory if allowances are made for absolute calibrations of the data. Calculations of plume emission according to some proposed mechanisms have been performed. It appears that production of OH by O atom attack on secondary H atoms in hydrocarbon fragments can result in substantial chemiluminescent emission from H_2O formed by subsequent reaction of the OH. Some semi-quantitative analogies between rocket exhaust flows and material releases in the upper atmosphere are discussed, and derivations directed toward comparing collision energy distributions at very high altitudes are presented.

FOREWORD

This research was supported by the Defense Advanced Research Projects Agency of the Department of Defense and was monitored by Air Force Cambridge Research Laboratories under Contract No. F19628-72-C-0006. This Second Semi-annual Technical Report covers the period from January 1, 1972, to June 30, 1972.

The author wishes to acknowledge the contributions of Drs. E. R. Fisher, J.A.L. Thomson, and I. Oppenheim through a number of stimulating discussions.

TABLE OF CONTENTS

		Page
Abstract		iii
Foreword		iv
Table of Contents		v
Figure Captions		vi
1.0	INTRODUCTION	1
2.0	MODELLING STUDIES	3
2.1	Comparisons with Experiment	3
2.2	Further Flow Field Calculations	5
2.3	Multistep V-V and V-T Processes	6
2.4	IR Chemiluminescence in Hydrocarbon/ Oxygen Systems	14
3.0	SIMULATION STUDIES	19
References		44
Figures		47

FIGURE CAPTIONS

1. Vibrational temperature of N_2 as a function of altitude in the ionosphere.

2. Cumulative radiant intensity of the "turbulent" Apollo S-II plume at 120 km in the H_2O ν_1 or ν_3 bands upstream of a given axial distance for two assumed values of the N_2 vibrational temperature according to the "two-step" V-V, V-T mechanism.

3. Cumulative production of vibrationally excited N_2 in the "turbulent" Apollo S-II plume at 120 km upstream of a given axial distance.

4. Cumulative radiant intensity of the laminar Atlas sustainer plume at 120 km in the H_2O ν_1 or ν_3 bands upstream of a given axial distance for the OH chemiluminescence mechanism. For curve I, OH is formed only by $O + H_2$; for curve II, the reaction $O + C_nH_{2n+2}$ also contributes. Turbine exhaust composition by moles is 26% H_2, 11% CO, 4% CO_2, 1.3% H_2CO, 2.6 % CH_4, 2.6% C_2H_6, 19.5% C_nH_{2n+2}.

5. Cumulative radiant intensity of the laminar Atlas sustainer plume at 120 km in the H_2O ν_1 or ν_3 bands upstream of a given axial distance for the OH chemiluminescence mechanism. Conditions as in Figure 4 except that CH_2O mole fraction is 0.65%, C_nH_{2n+2} mole fraction is 20.2%.

6. General structure of rocket exhaust plumes (a) and material releases (b) in the upper atmosphere at low ambient pressures. Continuum hydrodynamics assumed.

7. Coordinate system for describing rocket exhaust plume flow and interactions with the free stream.

8. Coordinate system for describing spherical releases and their interactions with ambient gas.

9. Surfaces of constant first collision energy between atmospheric molecules and released gases when the initial velocity of the released material is large.

1.0 Introduction

In the first semi-annual technical report on this contract,[1] we discussed a number of modelling studies of high-altitude (100 - 300 km) exhaust plume emission, predominantly in the near and middle infrared, and concentrating on processes taking place in the mixing region between plume gases and the atmosphere. It is generally believed that this part of the plume is responsible for the emission from large vehicle exhaust plumes measured by various means in the near infrared region. This belief has been confirmed for at least one vehicle by the recent ARPA-sponsored AFCRL measurements of the Apollo 14 and 15 S-II stages.[2] The outcome of the studies described in our earlier report was that there appeared to be no mechanism or set of mechanisms yet investigated which, when combined with rather detailed flow field calculations and the available information on rates or cross sections of the pertinent reactions and excitation processes, produces a calculated radiant intensity as large as that observed for the Atlas and Apollo vehicles.

During the period covered by the present report, we have continued these modelling studies. The activities have included a fairly detailed examination of the results generated in the first reporting period, a comparison of the fluid-dynamical part of the calculation with experimental data[3], and a re-ex-

amination of some of the chemistry and excitation mechanisms included in the models. The results of these investigations can be summed up as follows:

1. The results of the earlier modelling calculations appear reasonable, for the conditions examined.

2. The fluid-dynamical calculations agree reasonably well with experimental measurements.

3. The emission produced by chemi-excitation in the exhaust plumes of hydrocarbon vehicles is substantially increased when O atom reactions with unburned hydrocarbons are considered, and this mechanism could be responsible for a substantial portion of the radiant intensity of the Atlas plume.

A number of additional flow-field calculations have been performed; as yet, most of these have not been investigated for radiation produced.

In addition to the above work on the modelling studies, work has been initiated on other tasks in the contract. Revisions to the Exhaust Plume Phenomenology Handbook[4], prepared under a previous contract, have begun. We anticipate that a revised version of this Handbook, including available results from the ARPA Plume Physics Program, will be issued later this year. Studies of simulation of exhaust plumes have also been initiated. These studies are predominantly aimed at defining the degree of simulation of exhaust plume processes by atmospheric material releases.

These studies are discussed in greater detail in the following sections.

2.0 Modelling Studies

2.1 Comparisons with experiment:

As a means of validating a portion of the modelling activity conducted under the first half of the contract, we undertook a comparison between a flow field experiment conducted at Arnold Engineering Development Center[3] and a calculation conducted here. This calculation will be the subject of a separate report[5], so only the high points will be included here.

The experiment was conducted in Tunnel M of the Von Karman Gas Dynamics Facility and involved a simulated plume (represented by a jet of heated helium) mixing into a simulated free stream (represented by a surrounding flow of N_2). The forward portion of the plume is expected to be in the merged layer flow regime. Measured data include dynamic pressure (ρu^2) and species number densities (n_i) of N_2 and He in the mixing zone. There remains some question as to the absolute values of these quantities due to the numerous corrections necessary to reduce the data. In addition, rotational (T_R) and vibrational (T_V) temperatures of N_2 were measured, but the results for T_V are characteristic of reservoir conditions rather than those in the test section, and the values of T_R vary strongly with upper state J level and permit no easy interpretation.

The calculations were performed with the MULTITUBE and BOW codes for the specified experimental conditions. The effect of the forebody housing the helium nozzle is included, and laminar mixing of He and N_2 is assumed. Comparisons of the calculation with the experiment indicates that:

1. Good agreement with measured values of ρu^2 is obtained except within the shocks. (The codes assume the shocks to be discontinuities.)

2. Good agreement with the shape of the measured distributions of n_{He} is obtained (again excepting values at the shocks), but the magnitudes of the measured values tend to be 40-60% higher than the calculations. This discrepancy is thought to have to do with difficulties in reducing the data, which are measured by an electron-beam technique.

3. Good agreement with measured values of n_{N_2} is obtained at downstream stations. However, at the station closest to the nozzle, significant differences are observed on the jet side of the mixing layer, where the measured N_2 density is significantly higher than the calculated value. The reason for the discrepancy is not clear at present. If this increased mixing were accompanied by increased temperature spread, it could have a significant effect on plume emission in this region.

The comparison does not provide a conclusive validation of the calculation, because of questions regarding data reduction and influence of the forebody on the plume nose region. However, the semi-quantitative agreement obtained indicates that the calculation is at least reasonably correct, with the excep-

tion of the shocks themselves and the inner portion of the mixing zone close to the nozzle. A comparison of measured and predicted temperatures would be most desireable, but no comparison can be made at this time.

2.2 Further flow field calculations:

Since our last report, a number of additional calculations of Atlas and Apollo exhaust plume flow field calculations have been performed. These calculations (and those reported in the preceeding section) were made at the AEC Lawrence Laboratory in Berkeley, California, using the Laboratory's CDC 7600 computer. In addition to being of interest in their own right, these calculations allowed us to gain some experience with the Lawrence Laboratory system, which we expect to be using in most future work on this contract.

Computations performed included a laminar Atlas sustainer plume at 180 km, a "turbulent" sustainer plume at 120 km (using the same eddy viscosity model used in our previous Apollo calculation), and two laminar Apollo S-II plumes at 180 km, one at the minimum velocity at this altitude (essentially the orbital injection altitude) of 4.2 km/sec and one at the burnout velocity of 5.3 km/sec. Because of an input data error in the continuation of the "slow" Apollo calculation, only the first 3 km of this plume calculation is reliable. It was our intention to perform a

number of calculations of chemistry and excitation processes in these flow fields at our Detroit facility. However, a number of difficulties arose in transferring the taped output from these calculations to regular CDC tapes, and although these have now been solved we have as yet not undertaken any calculations of rate processes in these flow fields. We plan to do so in the next reporting period.

2.3 Multistep V-V and V-T processes:

In the previous report, we began calculations of the effects of multiple-step excitation processes upon plume emission. These processes involve the production of polyatomic molecules in states with large vibrational quanta, such as the ν_3 mode of H_2O, through lower-energy intermediate states, such as the H_2O ν_2 mode. The reason that such processes are of interest is that computations of plume flow fields indicate that most of the H_2O in the exhaust plume is cold. Available information upon the rates of direct excitation processes for the H_2O ν_1 and ν_3 modes (in the form of rate constants derived from thermally averaging Marriott's quantum-mechanical cross-sections[6]) indicates that these are slow at low temperatures. This behavior is associated with the size of the vibrational quantum which must be produced in the collision. As a result of the plume's being cool and the direct excitation rate's being slow, it is possible that an indirect ex-

citation mechanism involving two smaller quanta exchanged in two separate collisions may be faster than the single quantum, one-collision process.

The scaling arguments introduced in our previous report indicate that these multiple-collision processes should be less important at high altitude, since (at constant temperature) the volume-integrated rate should vary as $\rho^{1/4}$ to $\rho^{3/4}$, depending upon the rate of the second process. In addition, some comparative calculations of the rates of a particular two-step vibrational excitation process and the chemi-excitation process considered earlier indicated that, in the S-II plume at 120 km, there should not be substantial differences in total rates of production. The process considered was the V-T, V-V process

1. $H_2O + M \rightleftharpoons H_2O(\nu_2) + M$
2. $H_2O(\nu_2) \longrightarrow H_2O + h\nu_2 \quad (6.3\mu)$
3. $H_2O\ (\nu_2) + M \rightleftharpoons H_2O\ (\nu_1 \text{ or } \nu_3)$
4. $N_2 + M \rightleftharpoons N_2^{\dagger} + M$
5. $N_2^{\dagger} + H_2O\ (\nu_2) \rightleftharpoons H_2O\ (\nu_1 \text{ or } \nu_3) + N_2$
6. $H_2O\ (\nu_1 \text{ or } \nu_3) \longrightarrow H_2O + h\nu_{1 \text{ or } 3} \quad (2.7\mu)$

in which the V-V transfer in the 4th step is close to resonance and snould occur frequently. In the current reporting period, we have examined this process in greater detail; however, using

the rate data available to us, we find no great contribution to the radiant intensity from this mechanism.

Radiative losses from the H_2O ν_2 mode (step 2) are significant enough that this step introduces some stiffness into the system of differential equations giving the rates of these processes. In previous applications all rates were slow enough that no problems of this kind were encountered, and it became necessary to modify slightly the numerical integration procedure in the NONEQ code to treat this problem satisfactorily. In this exploratory work, we have adopted a procedure similar to that of Moretti,[7] though much simpler inasmuch as only one stiff step occurs.

We assume that the radiative depletion of the ν_1 and ν_3 modes is fast enough that we may neglect the reverse processes in steps 3 and 5. The rate of photon production (step 6) is then essentially the rate of production of H_2O molecules in the ν_1 or ν_3 modes, as all these molecules radiate immediately. This assumption causes us to overestimate the radiant intensity due to this process. Since the calculated intensity is low, this overestimate causes no problem. With these assumptions, the rates of production of H_2O (ν_2), H_2O (ν_1 or ν_3), and $N_2^\dagger$ are

$$\frac{d}{dt} x_{H_2O(\nu_2)} = k_{1,f}\, x_{H_2O}\, x_M - (k_{1,r}\, x_M + k_2 + k_{5,f}\, x_{N_2\dagger}) x_{H_2O(\nu_2)} \tag{2.1}$$

$$\frac{d}{dt} x_{N_2\dagger} = k_{4,f}\, x_{N_2}\, x_M - (k_{4,r}\, x_M + k_{5,f}\, x_{H_2O(\nu_2)}) x_{N_2\dagger} \tag{2.2}$$

$$\frac{d}{dt} x_{H_2O(\nu_1 \text{ or } \nu_3)} = k_{3,f}\, x_M\, x_{H_2O(\nu_2)} + k_{5,f}\, x_{H_2O(\nu_2)}\, x_{N_2\dagger} \tag{2.3}$$

Here terms involving M are to be interpreted as sums over all collision partners.

Let $x_{H_2O(\nu_2)} = x$, $x_{N_2\dagger} = y$, and $x_{H_2O(\nu_1 \text{ or } \nu_3)} = z$ and assume that the mole fractions of H_2O, N_2, and M are essentially unchanged by this set of processes. Then the above equations become

$$\frac{dx}{dt} = A - \left|B + Cy\right| x \tag{2.4}$$

$$\frac{dy}{dt} = D - \left|E + Cx\right| y \tag{2.5}$$

$$\frac{dz}{dt} = \left|F + Cy\right| x \tag{2.6}$$

where the coefficients A to F are slowly varying functions of time along a streamline. Since y also varies slowly (the N_2 vibrational relaxation times are long), over a small finite time interval we can replace y by y_o, its value at the beginning of the interval. Then

$$\frac{dx}{dt} = A - \left[B + Cy_o\right]x$$

and the solution for x at the end of an interval Δt is

$$x = \frac{A\left\{1 - e^{-(B + Cy_o)\Delta t}\right\}}{B + Cy_o} + x_o\, e^{-(B + Cy_o)\Delta t} \qquad (2.7)$$

When B is large, corresponding to significant radiative losses from the ν_2 mode, the second term dominates. Now if y changes by only a small amount in time Δt, substituting the second term from (2.7) in (2.5), letting $y = y_o$ on the right, and integrating between $t = 0$ and $t = \Delta t$ gives

$$y - y_o = (D - Ey_o)\Delta t - \frac{Cx_oy_o}{B + Cy_o}\left[1 - e^{-(B + Cy_o)\Delta t}\right] \qquad (2.8)$$

and in similar fashion we have

$$z - z_o = \frac{F + Cy_o}{B + Cy_o}\, x_o \left[1 - e^{-(B + Cy_o)\Delta t}\right] \qquad (2.9)$$

When radiative losses from the ν_2 mode are severe, and produce considerable stiffness in the equations, we may use Equations (2.7), (2.8), and (2.9) to calculate the changes in x, y, and z over a single step. When the radiative losses are minimal, there is no problem of stiffness and the straightforward numerical integration of Equations (2.1), (2.2), and (2.3) can be carried out as before.

We have applied this procedure to estimate the radiant intensity from the (turbulent) Apollo 15 plume due to this

mechanism at an altitude of 120 km. The flow field was computed in the previous reporting period. Rates of V-T processes involving the H_2O modes were taken from the calculations of Fisher,[6] who has thermally averaged Marriott's theoretical cross-section for a variety of processes. Using these data underestimates the production of $H_2O(\nu_2)$ in H_2O - H_2O collisions at the lower temperatures; however, it is difficult to extrapolate the experimental data, and the differences (about a factor of 5) between the theoretical and experimental rates for this process are not of great significance in view of the results of the calculation. Marriott has calculated[8] cross-sections for H_2O excitation in collisions with H_2 and H_2O only. These should be the faster processes wherever the concentrations of H_2 and H_2O are high. In the outer regions of the plume, excitation by collision with O, O_2, and N_2 is possible. The rates of excitation by O_2 and N_2 should be slow because of the greater mass of these molecules, but the rate of excitation by O - H_2O collisions may be important. In the absence of any theoretical or experimental information, we have assumed (as in our previous report) that these rates are identical to the H_2O - H_2O rates, for which the reduced mass of the collision pair is similar.

The N_2 V-T rates are derived from the correlation of Millikan and White.[9] These should be satisfactory for N_2 and O_2 collisions, but their use for H_2, H_2O, and O is question-

able. No information is available on relaxation of N_2 by H_2 or H_2O; however, the relaxation of the electronically similar CO molecule by H_2 is part of the data on which the correlation is based, and extension to N_2 appears reasonable. The relaxation of N_2 by O atoms is currently under study at Stanford Research Institute, but no results were available to us at the time these calculations were being done. We assume that the probability of transferring a vibrational quantum between N_2 and H_2O is 0.01 at all temperatures; no data are available, but on the basis of N_2 - CO_2 data this value would appear to be a somewhat higher estimate.

It is generally agreed that the vibrational temperature of N_2 is not in equilibrium with with the translational temperature at altitudes above 100 km. A recent calculation by Jamshidi and Kummler[10] (Figure 1) gives a value of approximately 750°K for T_{V,N_2} at 120 km. The translational temperature, according to the CIRA tables, is 355°K. In our calculations for the radiant intensity of the S-II stage, we have used T_{V,N_2} = 750°K and T_{V,N_2} = 2000°K. The higher temperature corresponds roughly to a calculation by Walker[11] assuming that all energy deposited in the ^1D state of atomic oxygen by solar photodissociation of O_2 (Schumann-Runge continuum) is channeled into $N_2\dagger$.

Results of these calculations are shown in Figure 2. Here we show cumulative radiant intensity as a function of

axial distance behind the vehicle for the two values of T_{V,N_2}. As expected, the calculated intensity varies strongly with ambient vibrational temperature. That it does not vary even more strongly is a consequence of excitation and de-excitation of $N_2\dagger$ in the shock layer. At a value of T_{V,N_2} = 750°K, additional $N_2\dagger$ is produced in the forward 3 km of the plume shock layer; however, at T_{V,N_2} = 2000°K, relaxation processes in the shock layer actually decrease the amount of $N_2\dagger$, since most of the shock layer is cooler than the ambient vibrational temperature. The rates of production are shown (again cumulatively as a function of downstream distance) in Figure 3 . The slope of these curves gives the local production rate per unit length of the plume shock layer.

The values of total radiant intensity from the H_2O ν_1 and ν_3 bands are 1.5×10^4 watts/steradian at T_{V,N_2} = 750°K and 3.5×10^4 watts/steradian at T_{V,N_2} = 2000°K. These values would be up to a factor of 5 higher if we increased the rate constants of step 1 to bring the H_2O (ν_2) production rate by collisions with H_2O into agreement with experimental values. Recall, however, that most of the other assumptions that we made tended to favor the production of 2.7μ radiation from this system. It is therefore difficult to ascribe the S-II emission to this mechanism unless one or more of the important rate constants were in error by a factor of 100.

2.4 IR chemiluminescence in hydrocarbon/oxygen systems:

In our previous report, we presented results for calculations of possible IR chemiluminescence from the Atlas sustainer and Apollo S-II plumes. These calculations were based upon a reaction sequence

$$H_2 + O \rightleftharpoons OH + H$$

$$OH + R\text{-}H \longrightarrow R\cdot + H_2O\dagger$$

where R is anything from an H atom to a hydrocarbon chain and unit quantum yield is assumed in the second step. The results of the calculations were generally negative; on the basis of available rate data, the production rate of excited H_2O by this mechanism was quite low.

This conclusion was surprising in view of earlier approximate calculations by Fisher,[12] who had indicated that, for quantum yields near unity, the production rate should be high. As a consequence, part of our effort during this reporting period has been devoted to checking the numerical integration procedure in various ways and to determining why our numerical calculations differ from Fisher's approximate calculation. We have as yet found no indication that the numerical calculations were incorrect. In general, any approximations made tend to favor the production of excited H_2O rather than to limit its production. Fisher's calculation differs from the current calculation in three ways: 1) he assumed a higher

value for the rate constant of the O + H_2 reaction than that currently favored (Leeds compilation); 2) the extrapolation which he introduced to extend the data from the two streamlines available to him at that time overestimates the total reaction; and 3) he assumed the concentration of CH_2O, which turns out to be the most important R-H species in hydrocarbon/oxygen plumes because of the high value for the OH + CH_2O rate constant, to be about 2% by moles everywhere in the combustion gas, whereas in the current calculation it is assumed to be this high only in the turbine exhaust gases.

It is difficult to assign mechanistic implications to these calculations for hydrocarbon/oxygen systems because it has been necessary to guess the amounts of R-H species (other than H_2) which are present in the plume. Ther are no available measurements of these concentrations. All available calculations are based upon assumptions of local microscopic homogeneity and thermochemical equilibrium in the combustion chamber, and while these assumptions lead to reasonable values of exit conditions and major species concentrations, they are wholly inadequate for predicting minor species levels. Another serious defect is that the reaction system is incomplete. A potentially large number of important reactions was purposely excluded from the calculation. Hydrocarbon combustion is a very complex process, and to include all possible reactions in a calculation of radiant intensity would prove extremely

lengthy and expensive. (On the order of 1000 different reactions occur in the oxidation of a gasoline-fraction alkane.[13]) For most of these reactions, rate data are unavailable and must be estimated; thus increasing the complexity of the calculation does not necessarily increase its accuracy. Our decision to limit the calculation to essentially the above sequences was based upon the outcome of the approximate calculations, which suggested that this sequence was sufficient to explain observations. It now appears that this assumption is incorrect, and that the reaction scheme should be expanded.

Fisher and Kummler[14] have reviewed hydrocarbon oxidation processes as part of studies directed at the interpretation of flow-tube experiments in IR chemiluminescence. The major features of the combustion process in the presence of significant amounts of O atoms are the following: A significant contribution to the total OH production rate is the attack of O atoms upon secondary hydrogen atoms in aliphatic hydrocarbons:

$$O + R_1\text{-}CH_2\text{-}R_2 = OH + R_1\text{-}\dot{C}H\text{-}R_2$$

This reaction is generally nearly thermoneutral, so that no excited products are expected. The radical can react with either O or OH to form an olefin; if R_2- is $R_3\text{-}CH_2$- , then

$$R_1\text{-}\dot{C}H\text{-}CH_2\text{-}R_3 + O \longrightarrow R_1\text{-}CH{=}CH\text{-}R_3 + OH$$

$$R_1\text{-}\dot{C}H\text{-}CH_2\text{-}R_3 + OH \longrightarrow R_1\text{-}CH{=}CH\text{-}R_3 + H_2O$$

Enough energy is liberated in these reactions to excite the products. The olefin in turn can react with O to form an aliphatic radical and the formyl radical:

$$R_1\text{-}CH{=}CH\text{-}R_3 + O \longrightarrow R_1\text{-}\dot{C}H\text{-}R_3 + CHO$$

Then the formyl radical can undergo reactions with O to give CO and OH, with OH to give O and formaldehyde, or with H_2O to give OH and formaldehyde. A series of reactions involving O, OH, H_2, and CO completes the system.

We are currently coding a lumped-parameter reaction scheme for this sequence of processes. We expect to report on the results of these calculations in our next semi-annual report. While the scheme was being formulated, we performed an approximate calculation in which we merely added to the reaction scheme used in our previous Atlas sustainer calculations the reaction

$$n\text{-}C_5H_{12} + O \longrightarrow C_5H_{11} + OH$$

assuming that all the hydrocarbons in the sustainer turbine exhaust flow were normal pentane. The rate constant measured by Herron and Huie[15] is $8 \times 10^{13}\ e^{-2320/T}\ cm^3/mole\ second$. We attempted to account for the fact that there is a chain of subsequent processes by ignoring the depletion of the hydrocarbon species in this reaction. Results of this calculation for slightly different initial formaldehyde concentrations in

the turbine gas are shown in Figures 4 and 5, together with results from a similar calculation without this reaction. Including OH production by this process greatly increases the potential level of IR chemiluminescence in the sustainer plume, and makes this mechanism again appear a likely contributer to the overall radiant intensity in the OH and H_2O vibration-rotation bands. More detailed calculations, including variation of the assumptions about the concentrations of unburned fuel and combustion intermediates, are necessary before we can draw any more firm conclusions.

This mechanism will not contribute to emission from hydrogen-oxygen plumes such as those of the Apollo S-II or Centaur vehicles. It may contribute to emission in amine-fueled vehicles, although it seems unlikely that many long-chain hydrocarbons are produced in the combustion of methylated hydrazines. There may be analogous reactions in substituted hydrazine systems; we are currently conducting a literature survey to discover whether this is the case.

3.0 Simulation Studies

During this reporting period we initiated studies of the simulation of high-altitude exhaust plume emission in ground facilities and in high-altitude atmospheric releases. These studies are aimed at simulating the plume-atmosphere mixing region rather than the plume core, which can be reproduced (except for very large engines) in ground facilities. There seem to be two reasons for wanting to perform a simulation experiment:

1) The number of processes which could contribute to the plume emission in the near IR is large, and the processes responsible have as yet not been clearly identified. A simulation experiment offers (at least in concept) the chance to repeat the experimental conditions, to ask more detailed questions about the state of the plume as a function of position, and, by changing the experimental conditions, to alter the rates of competing processes to determine which are most significant. In particular, it is desireable to find out whether any important effects have been left out of the calculation.

2) The models developed for predicting plume emission are complicated, and verifying the computational results is difficult. A simulation experiment offers the chance of exercising the models against a representation of reality in which more detailed comparisons are possible than are available from most field data.

Both ground and atmospheric simulation experiments have some advantages and some disadvantages in terms of achieving these objectives.

The advantages of a ground simulation experiment are its controllability, reproducibility, capacity to accept changes in experimental conditions, and the fact that a wide variety of diagnostic measurements (local and remote) can be performed. One can simulate both proper ratios of binary reaction rates and plume fluid dynamics at the same time if the product of engine thrust and ambient pressure is held constant and all temperatures, velocities, and pertinent compositions are reproduced. However, one cannot simulate effects depending upon the ratio of the radiative lifetime to a characteristic collision time (or flow time) in the infrared if one scales the thrust by more than about one order of magnitude. The simulation can break down in either of two ways:

1) The increased pressure can result in the radiation's being forced toward the equilibrium limit, in which the local emission is independent of the processes producing the excited states and the experiment tells one nothing about these processes.

2) The decreased length means that, even if radiative decay is the predominant de-excitation mechanism, excited molecules can be convected into downstream parts of the flow field before they are de-excited. Since the radiation is no longer characteristic of local conditions, its interpretation is difficult.

In either case, the experiment cannot be scaled back to the real plume conditions without considerable effort. Other difficulties arise when one attempts to include full chemical simulation of the atmosphere (degree of oxygen dissociation, N_2 vibrational temperature) and the nozzle exit gases (combustion intermediates).

In the ultraviolet and visible the difficulties with the radiative lifetime do not exist, since the lifetimes of all the upper states of interest are so short that $\tau_R/\tau_C << 1$ in both the real and the simulated flows. The major problems are associated with reproducing the nozzle exit chemistry.

In the current reporting period our activity has been mostly concerned with defining the possibilities of partial simulation of exhaust plumes by means of atmospheric releases of material. The release could take several forms, but the end result is essentially a cloud of material which interacts with the ambient atmosphere in a manner which under some conditions closely mimics the interaction of the plume with the atmosphere. The morphology of the two flows (in the continuum regime) is shown in Figure 6 .

We assume that the release is either cylindrically or spherically symmetric, that its initial velocity is zero, and that the container is removed at $t = 0$. The released gas expands in a manner determined by the initial distribution of

density and the value of γ behind a front which, in vacuo, would attain a speed of $2a_o/(\gamma - 1)$, where a_o is the initial speed.[16] (The density and pressure at this front are zero.) This front is the analog of the limiting line for the Prandtl-Meyer expansion of the plume gas. As the released gas expands, its dynamic pressure decreases. When the dynamic pressure of the released gas becomes comparable to the ambient pressure, the released gas will be decelerated by the surrounding atmosphere. Since most of the expanding gas will become supersonic if the expansion ratio is large, the decelaration will occur through a shock wave which propagates inward from the contact surface into the expanding gas cloud. This shock wave will eventually reach the center or axis of the cloud and be reflected (regularly - there is no analog of the Mach disc). Since the released gas will, if initially hot, expand at velocities supersonic with respect to the ambient atmosphere, the ambient gas just outside the contact surface will be swept outward at a supersonic velocity and a shock wave will form in the ambient gas (just as in a shock tube). In general, the contact surface will overshoot its equilibrium position and oscillate around this position until the internal shock reflects several times off the center or axis and the contact surface. The equilibrium radius is proportional to $(E_o/P_\infty)^{1+j}$, where E_o is the initial energy (per unit length in the cylindrical case) of the released material, P_∞ is ambient pressure, and j is a metric

coefficient (1 for cylindrical and 2 for spherical geometry). Viscous transport occurs across the interface, which can be Rayleigh-Taylor unstable if the released gas at the interface is more dense than the shocked air (normally the case, since the released gas is relatively cool).

In the exhaust plume (cylindrical geometry) a roughly similar series of processes takes place. There is, in fact, a direct analogy between flows in an exhaust plume with high exit and free-stream Mach numbers and a cylindrical release. The analogy becomes exact over the outward-moving portions of the flows (forward part of the plume and early part of the release) in the limiting case that all Mach numbers are high, all flow angles are small (but $M\sin\phi \ll 1$), and the jet and free-stream limiting velocities are identical. In this case the two flows may be connected through a simple Galilean transformation $x = u_\infty t$. (The aerodynamicist calls this the "hypersonic equivalence principle.")

In practical situations, the conditions for exact analogy are not fulfilled. As we noted parenthetically above, the plume flow will form a Mach disc and the release flow cannot. If the Mach number at the nozzle exit is only moderately large, the Prandtl-Meyer turning angle is usually large enough that the air shock is detached at the plume nose, and in all practical cases the small-angle criterion is not fulfilled. In addition, a point release would usually be spherical (or some

approximation thereto) and the exact analogy breaks down in any case because of different divergence terms in the equations of motion. Nonetheless, there may remain a fair degree of similarity between the two flows, and in particular for cases when vehicle velocity and plume velocity are closely matched the development of a stationary release as a function of time provides a semi-quantitative analog to the development of a plume as a function of downstream distance.

The quantity of material to be released is a question of considerable importance, since it sizes the carrier vehicle required. If we take the approach that we maintain constant altitude (to get identical atmospheric conditions) and reproduce the plume Knudsen number based upon its equilibrium radius with the similar Knudsen number of a stationary spherical release (to reproduce mixing phenomena or molecular distribution functions), then the amount of material can be determined approximately as follows: The equilibrium radius of the plume is

$$r_p \sim 0.1 \sqrt{F/P_\infty} \tag{3.1}$$

and of the release is

$$r_R \sim (E_o/P_\infty)^{1/3} \ . \tag{3.2}$$

We assume that the velocity of the plume-generating vehicle is equal to the limiting velocity of the plume gases u_p. Then

the temperatures in the plume are, for the most part, governed by the nozzle exit temperature (which provides the energy which will be converted into kinetic energy of lateral expansion) and the air temperature. The rocket thrust is

$$F \approx \dot{m}\, u_p \tag{3.3}$$

and the initial energy of the released material is

$$E = \frac{1}{2\gamma}\, \dot{m}\, u_R^2 \tag{3.4}$$

where u_R is the limiting steady-flow velocity of the released gas. Then if P_∞ is the same in both cases and $r_p/r_R \approx 1$, we have

$$0.1(\dot{m}\, u_p/P_\infty)^{1/2} \approx (m\, u_R^2/2\gamma P_\infty)^{1/3}$$

or

$$m \approx 0.002\gamma(\dot{m}^3\, u_p^3/P_\infty u_R^4)^{1/2} .$$

For a rocket with 10^5 lb thrust at an altitude of 180 km,

$$\dot{m} \approx 1.5 \times 10^5 \text{ gm}$$

$$u_p \approx 3.5 \times 10^5 \text{ cm/sec}$$

$$P_\infty \approx 2 \times 10^{-3} \text{ dynes/cm}^2$$

Assuming that the released gas is initially at the nozzle exit temperature, and taking this temperature as 1/4 the chamber temperature, gives $u_R \approx 1/75 \times 10^5$ cm/sec. Then with $\gamma = 1.4$, we have

$$m \approx 2.8 \times 10^{-3} (3.38 \times 10^{15} \times 4.3 \times 10^{16} / 2 \times 10^{-3} \times 9.4 \times 10^{20})^{1/2}$$

or

$$m \approx 2.5 \times 10^{4} \text{ gm} \approx 55 \text{ lb}$$

This appears to be within the lifting capability of available sounding rockets, even if a sizeable extra factor is included for storage and controls.

It is not necessary to perform the release at zero velocity. By releasing the material with appreciable velocity, one obtains a higher collision energy between release and atmospheric molecules. However, one loses both symmetry (since forward and rear portions of the released gas feel a different effective pressure) and the qualitative analogy to the development of a thrusting plume. The forward part of the release qualitatively resembles a retro plume during a portion of the expansion. Velocities available depend upon the choice of carrier vehicle and range from essentially zero (sounding rockets) to about 7 km/sec (piggyback on large missile).

Since the purpose of performing the release is to learn about chemistry and excitation processes in high-altitude plumes, one hopes that the distribution of collision energies in a release can be tailored to correspond closely to the distribution in a plume. In this report we have begun in-

vestigating the conditions under which this correspondence exists. We intend to examine both high-altitude plumes, where the flows are in a nearly free-molecular condition (after the initial portion of the expansion), and moderately low-altitude plumes (100-150 km), where the flows are in the continuum regime. In the low-altitude situation, we will employ a new one-dimensional unsteady flow code developed over the past year at Wayne State University for the release and compare the results to MULTITUBE calculations of the plume flow. In the high-altitude situation, we adopt a first collision approach, and the remainder of this section is concerned with the formulation of this comparison at high altitudes.

We assume that the rocket engine generating the exhaust plume and the mass of released material are large enough that the limiting density distribution in each flow is achieved as a result of essentially inviscid expansions. The ambient mean free path λ_∞ is taken to be very long, so that the flow patterns established in the expansions persist to large distances or times. At some distance r^* or time t^* the expanding plume or cloud becomes itself so rarefied that it is highly permeable by atmospheric molecules. (We assume that λ_∞ is considerably greater than the dimensions of the plume or cloud when this occurs.) Under these conditions the initial collisions between injected and atmospheric molecules can

be treated as rare and independent events, and the velocity and density distributions of the bulk of the injected material are unaffected by the presence of ambient molecules. Thus these distributions are those appropriate to flow into a vacuum. It is these "first collisions" which are of especial interest in problems where the reaction or excitation cross-section is a strongly increasing function of energy.

For an exhaust plume expanding into a vacuum, the asymptotic density distribution, in spherical polar coordinates (r,θ,ϕ) centered at the nozzle (which is very small compared with the dimensions r^* of the interaction volume) and with the z-axis or north pole pointing along the thrust vector (Figure 7), is approximately

$$\rho = \frac{F}{I_{sp}\, u_\infty r^2} \cdot a(\gamma) f(\theta) , \qquad (\theta < \theta_\infty) \qquad (3.5)$$

where $a(\gamma)$ is determined by mass conservation and $f(\theta)$ is conveniently either

$$f = \left(1 - \frac{\theta}{\theta_\infty}\right)^{2/\gamma-1} \qquad (3.6a)$$

or

$$f = \cos^{2/\gamma-1}\left(\frac{\pi}{2}\,\frac{\theta}{\theta_\infty}\right) , \qquad (3.6b)$$

where θ_∞ is the limiting angle for a Prandtl-Meyer expansion at the nozzle lip. The effects of nozzle wall boundary layer

will be neglected. Here also u_∞ is the limiting velocity for a steady flow, $u_\infty = \sqrt{2H}$ where H is the total enthalpy. The velocity distribution is $\vec{u}(\theta) = u_\infty \hat{r}(\theta)$ for $\theta \leq \theta_\infty$.

For an initially uniform gas cloud expanding into a vacuum, the asymptotic density distribution can be taken from an approximate formulation given by Hubbard:[17]

$$\rho = D(\gamma,j) \frac{m}{(a_o t)^{j+2}} \left[1 - \left(\frac{R}{u_{max} t}\right)^n\right]^{B(\gamma,j)} \qquad (3.7)$$

where R is radial distance from the center of the cloud, t is time, j is a metric coefficient (equal to 0, 1, or 2 as the geometry is planar, cylindrical, or spherical), m is the mass released (per unit area or length in the case of a planar or cylindrical flow), $a_o = \sqrt{(\gamma-1)H}$ is the initial sound speed, and

$$u_{max} = 2\sqrt{H/(\gamma-1)} \qquad (3.8)$$

is the speed of the cloud boundary. The coefficients D and B are given by the mass conservation requirement

$$D = \left(\frac{\gamma-1}{2}\right)^{j+1} \left(\frac{n}{j+1}\right) \frac{\Gamma\left(B+2+\frac{j+1-n}{n}\right)}{\Gamma(B+1)\Gamma\left(1+\frac{j+1-n}{n}\right)} \qquad (3.9)$$

and the energy conservation requirement

$$D = \left(\frac{\gamma-1}{2}\right)^{j+2} \left[\frac{n}{\gamma(\gamma-1)}\right] \frac{\Gamma\left(B+2+\frac{j+3-n}{n}\right)}{\Gamma(B+1)\Gamma\left(1+\frac{j+3-n}{n}\right)} \qquad (3.10)$$

The velocity distribution is $\vec{u}(\vec{R},t) = \vec{R}/t$ for $|\vec{R}| < u_{max}t$.

Equations (3.9) and (3.10) must be supplemented by an additional equation in order to determine the values of all three quantities n, B, and D. In the planar case, an exact solution to the expansion problem is available, and in this solution the asymptotic results give

$$n = 2$$

$$B = \frac{3 - \gamma}{2(\gamma - 1)}$$

$$D = \frac{\gamma - 1}{\sqrt{\pi}} \Gamma\left(N + \frac{1}{2}\right) \Big/ \Gamma(N)$$

where

$$N = \frac{\gamma + 1}{2(\gamma - 1)} \quad .$$

In the cylindrical and spherical cases no such solution exists, and one must look to numerical solutions for assistance. Hubbard has chosen to fit the value of n to numerical calculations for the cylindrical case and to determine the values of B and D by Equations (3.9) and (3.10). The value of n chosen is

$$n = 2 + j \frac{\gamma(\gamma - 1)}{2\gamma - 1} \quad .$$

The maximum velocity is considerably larger than the limiting velocity u_∞ in a steady expansion, by the ratio

$$\frac{u_{max}}{u_\infty} = \sqrt{\frac{2}{\gamma - 1}} \quad . \qquad (3.11)$$

In the unsteady expansion, work is done on the gas at the leading edge of the expansion by the gas behind it, so that a transfer of energy occurs from gas toward the center of the cloud to gas at its edge. In the steady expansion, there is no leading edge, so that each element of gas not only has work done on it by gas upstream from it, but also does work on downstream gas. The average velocity of the expanding cloud is

$$u_{av} = \sqrt{2E} = \sqrt{2H/\gamma} = u_\infty \sqrt{1/\gamma} \qquad (3.12)$$

since energy is conserved.

The interaction of the atmosphere with the plume gases is best described in a coordinate system moving with the vehicle. If the vehicle velocity $\vec{V}$ is large compared with ambient thermal velocities, ambient molecules impinge upon the plume along essentially parallel trajectories with velocities $-\vec{V}$. The highly expanded plume gases are also hypersonic, so that a first collision takes place with a relative velocity

$$\vec{v}_r = u_\infty \hat{r} - \vec{V} , \qquad (3.13)$$

where $\hat{r}$ is a unit radial vector and the origin of coordinates is at the engine.

If the molecules are hard spheres, then the fraction of molecules penetrating the plume to a depth S along any individual trajectory is

$$\tau = \exp\left\{-\int ds' \frac{n\sigma v_r}{V}\right\} . \qquad (3.14)$$

For a thrusting vehicle at zero angle of attack, we consider that the trajectories are lines parallel to the axis and consider penetration to a distance z behind the axis. The integral in the exponent then becomes

$$\int_{-\infty}^{z} dz' \frac{n\sigma v_r}{V} = \frac{F\sigma N_{av}}{\bar{M} I_{sp} u_\infty V Z \tan\theta} \int_{\theta}^{\theta_\infty} d\theta' f(\theta') \sqrt{V^2 + u_\infty^2 - 2Vu_\infty \cos\theta'} \qquad (3.15)$$

for any angle $\theta = \tan^{-1}(r_o/z)$ where r_o is the distance from the axis of the trajectory. For a retrofiring vehicle, an identical expression results except that the integral is taken from zero to θ.

The number of first collisions per unit volume at a point in the plume given by particular values of z and θ is

$$\frac{d\mathring{N}}{dV} = n_\infty \tau \nu_{c,p} = n_\infty \tau n\sigma v_r \qquad (3.16)$$

where n_∞ is the ambient density and $\nu_{c,p}$ is the frequency of collision of an ambient molecule with plume molecules. The total number of such collisions between z and z +dz is

$$\frac{d\mathring{N}}{dz} dz = 2\pi \int_0^\infty dr\, r \frac{d\mathring{N}}{dV} dz = 2\pi z^2 \int_0^{\theta_{max}} d\theta \frac{\tan\theta}{\cos^2\theta} \frac{d\mathring{N}}{dV} dz$$

where θ_{max} is the lesser of θ_∞ and $\pi/2$.

The collision energy depends only on $\theta \left[E = \frac{1}{2} \mu v_r^2(\theta)\right]$. The rate at which plume molecules between z and z + dz undergo first

collisions with energies between E and E + dE is

$$\frac{d}{dE}\left(\frac{d\mathring{N}}{dz}\right) dE\, dz = \frac{d}{d\theta}\left(\frac{d\mathring{N}}{dz}\right)\left(\frac{dE}{d\theta}\right)^{-1} dE\, dz$$

where

$$\frac{dE}{d\theta} = \frac{1}{2}\mu V u_\infty \sin\theta$$

and

$$\frac{d}{d\theta}\left(\frac{d\mathring{N}}{dz}\right) = 2\pi z^2 \frac{\tan\theta}{\cos^2\theta} n_\infty \tau n\sigma v_r$$

$$= 2\pi \tan\theta \frac{n_\infty F N_{av} \sigma}{\bar{M} I_{sp} u_\infty} f(\theta) \sqrt{V^2 + u_\infty^2 - 2Vu_\infty \cos\theta}$$

so that

$$\frac{d}{dE}\left(\frac{d\mathring{N}}{dz}\right) = \frac{4\pi F N_{av} \sigma}{\bar{M} I_{sp} u_\infty^2 V\mu} \frac{f(\theta)}{\cos\theta} \tau(z,\theta) v_r(\theta) \qquad (3.17)$$

with $\theta = \theta(E)$.

The distribution of energies of the entire plume is obtained by integrating Equation (3.17) over z:

$$\frac{d\mathring{N}}{dE} = \frac{4\pi F N_{av} \sigma}{\bar{M} I_{sp} u_\infty^2 V \mu} \frac{f(\theta)}{\cos\theta} v_r(\theta) \int_{z_1}^{z_2} dz\, \tau(z,\theta)$$

Since z in principle varies between $\pm\infty$, the integral will diverge unless finite limits are put on it. These can be chosen to be the limits of the field of view of the observing instrument.

Since one is most interested in high-altitude plumes with an appreciable velocity with respect to the atmosphere,

the release connected with such a plume would most reasonably be performed with an appreciable velocity. We again adopt a a cylindrical coordinate system with the origin at the center of the release and the z-axis pointing in the direction parallel to the flux of incoming molecules (Figure 8). We consider times short with respect to $\lambda_\infty u_{max}$ but long with respect to the time required to establish the asymptotic density distribution given by Equation (3.7).

Consider an elemental volume consisting of an annulus of thickness dr and width dz at a distance r from the z-axis. Let $n(r,z,t)$ be the local density of uncollided atmospheric molecules at time t, $n_R(r,z,t)$ the local density of released molecules, v_∞ the velocity of the released gas with respect to the atmosphere, $v_r(r,z,t)$ the relative velocity between released and atmospheric molecules, and σ the collision cross-section. The rate of accumulation of uncollided atmospheric molecules within this elemental volume is

$$\frac{\partial n}{\partial t} 2\pi r \, dr \, dz \quad .$$

The rate flow of uncollided atmospheric molecules into this volume is

$$n(z,r,t)v_\infty \, 2\pi r \, dr$$

and the rate of flow out of the volume is

$$n(z+dz,r,t)v_\infty \, 2\pi r \, dr \quad .$$

The rate at which collisions occur is

$$n(z,r,t)n_R\sigma\ v_r\ 2\pi r\ dr\ dz\ .$$

By setting accumulation equal to flow in less flow out less collision rate, and using the usual Taylor series expansion for $n(z+dz)$, we arrive at the following partial differential equation for $n(z,r,t)$:

$$\frac{\partial n}{\partial t} + \frac{\partial n}{\partial z}\ v_\infty + n(r,z,t)\sigma\ v_r(r,z,t)n_R(r,z,t) = 0 \qquad (3.18)$$

Here the relative velocity is

$$v_r = \left[v_\infty^2 + (r^2 + z^2)/t^2 - 2v_\infty\sqrt{r^2 + z^2}/t\ \cos\theta\right]^{1/2} \qquad (3.19)$$

with

$$\theta = \cos^{-1}\frac{z}{\sqrt{r^2 + z^2}}$$

and the local number density of released-gas molecules is

$$n_R = \frac{m}{\bar{M}(a_o t)^{j+2}}\ D\left[1 - \left(\frac{r^2 + z^2}{u_{max}^2 t^2}\right)^n\right]^B \qquad (3.20)$$

The complicated form of the third term makes a general solution of Equation (3.18) difficult to obtain. Two special-case solutions can readily be found. First, if v_∞ is zero, the equation reduces to an ordinary differential equation for $n(t)$ at given r and z, with solution

$$\underset{\sim}{n}(t;r,z) = \underset{\sim}{n}_\infty \exp\left\{-\int_o^t n_R\sigma\left(\sqrt{r^2 + z^2}/t\right)dt\right\} = \underset{\sim}{n}_\infty\varepsilon(R,t) \qquad (3.20)$$

where $R = \sqrt{r^2 + z^2}$. We can write

$$\varepsilon = \exp\left\{ - D \frac{m N_{av}}{\bar{n} a_o^{j+1}} R \int_{R/u_{max}}^{t} dt' t'^{-(2+j)} \left[1 - \left(\frac{r}{u_{max} t'} \right)^n \right]^B \right\} \quad (3.21)$$

and in the case of a spherical release (j = 2) the integral becomes

$$\frac{1}{2n} \left(\frac{u_{max}}{r} \right)^3 \left[\frac{\Gamma\left(\frac{1}{2}\right)\Gamma(B+1)}{\Gamma\left(B + \frac{3}{2}\right)} - \beta_x\left(\frac{1}{2}, B+1\right) \right] \quad (3.22)$$

where $\beta_x(a,b)$ is the incomplete Beta Function and $x = (r/u_{max}t)^{2n}$. With $\underset{\sim}{n}$ thus expressed as a function of space and time, we can proceed to evaluate the collision energy distribution as follows:

At any point, the rate of first collision per unit volume is

$$\frac{d\dot{N}}{dV} = \varepsilon(R,t) \underset{\sim}{n}_\infty \underset{\sim}{n}_R(R,t) \sigma \frac{R}{t}$$

and the entire rate integrated over the volume of released material is

$$\dot{N}(t) = 4\pi \underset{\sim}{n}_\infty \sigma \int_0^{u_{max}t} dR\, R^3\, \varepsilon(R,t) \underset{\sim}{n}_R(R,t)/t$$

$$= 4 \frac{n_\infty \sigma m N_{av}}{\bar{M} a_o^3 t^4} D \int_0^{u_{max}t} dR\, R^3 \varepsilon(R,t) \left[1 - \left(\frac{R}{u_{max}t} \right)^n \right]^B \quad (3.23)$$

The collision energy is $\frac{1}{2} \mu R^2/t^2$. The rate at which released and atmospheric molecules undergo first collisions at time t with energies between E and E + dE is

$$\left(\frac{\partial \dot{N}}{\partial E} \right)_t dE = \left(\frac{\partial \dot{N}}{\partial R} \right)_t \left(\frac{\partial E}{\partial R} \right)_t^{-1} dE$$

where

$$\left(\frac{\partial E}{\partial R}\right)_t = \mu R/t^2$$

and for a spherical release

$$\left(\frac{\partial \dot{N}}{\partial R}\right)_t = 4\pi \frac{\underset{\sim}{n}_\infty \sigma m N_{av}}{\bar{M} a_o^3 t^4} R^3 \epsilon(R,t) D\left[1 - \left(\frac{R}{u_{max} t}\right)^n\right]^B$$

and thus

$$\left(\frac{\partial \dot{N}}{\partial E}\right)_t = 4\pi \frac{\underset{\sim}{n}_\infty \sigma m N_{av}}{\bar{M} \mu a_o^3 t^2} R^2 \epsilon(R,t) D\left[1 - \left(\frac{R}{u_{max} t}\right)^n\right]^B \qquad (3.24)$$

The second situation in which an easy solution is found is at times long enough that $\underset{\sim}{n}_R$ is very small. Then the third term in Equation (3.18) vanishes and the solution for $\underset{\sim}{n}$ becomes $\underset{\sim}{n} \equiv \underset{\sim}{n}_\infty$ everywhere. Then the local first collision frequency is simply

$$\frac{d\dot{N}}{dV} = \underset{\sim}{n}_\infty \underset{\sim}{n}_R \sigma v_r \qquad (3.25)$$

with

$$v_r(r,z,t) = \left[v_\infty^2 + \frac{r^2+z^2}{t^2} - 2v_\infty \frac{z}{t}\right]^{1/2} \quad (r^2+z^2) < u_{max}^2 t \qquad (3.26)$$

and the volume-integrated rate is

$$\dot{N} = 4\pi \underset{\sim}{n}_\infty \sigma \int_0^{u_{max}t} r\, dr \int_0^{\sqrt{u_{max}t - z^2}} dz\, \underset{\sim}{n}_R(r,z,t)\, v_r(r,z,t) \qquad (3.27)$$

The collision energy is

$$E = \tfrac{1}{2} \mu v_r^2 = \tfrac{1}{2} \mu \left[v_\infty^2 + \frac{r^2+z^2}{t^2} - 2v_\infty \frac{z}{t}\right] \qquad (3.28)$$

or, alternatively,

$$E = \frac{1}{2}\mu\left[v_\infty^2 + \frac{R^2}{t^2} - 2v_\infty \frac{R}{t}\cos\theta\right]^2 \qquad (3.29)$$

Likewise, we can rewrite $\dot{N}$ in terms of R and θ as

$$\dot{N} = 2\pi \underset{\sim}{n}_\infty \sigma \int_0^{u_{max}t} dR\, R^2 \int_0^\pi d\theta \sin\theta\, \underset{\sim}{n}_R(R,t) v_r(R,\theta,t) \,. \qquad (3.30)$$

We can now rewrite both (3.29) and (3.30) to remove the explicit time dependence, using the substitution $\eta = R/u_{max}t$

$$E = \frac{1}{2}\mu\left[v_\infty^2 + u_{max}^2 \eta^2 - 2v_\infty u_{max}\eta\cos\theta\right] \qquad (3.31$$

and

$$\dot{N} = 2\pi D \frac{m\, \underset{\sim}{n}_\infty \sigma u_{max}^2}{\bar{M} a_o^3} \int_0^1 d\eta\, \eta^2\left[1-\eta^n\right]^B \cdot$$

$$\int_0^\pi d\theta \sin\theta \left[v_\infty^2 + u_{max}^2 \eta^2 - 2v_\infty u_{max}\eta\cos\theta\right]^{1/2} \qquad (3.32)$$

where we have used (3.20). This development shows that the total number of collisions is constant in time, since it depends upon a density which varies as t^{-3} and a volume which varies at t^3.

In this case the collision energy depends upon both η and θ (or r and z), so that determining $d\dot{N}/dE$ becomes more complicated. The surfaces of constant E are ellipsoids of revolution about the z-axis (Figure 9). These ellipsoids either will or will not intersect the sphere $\eta = 1$ depending upon the values of E,

v_∞, and u_{max}. The values of E of interest range between

$$E_{min} = \min\left[0, \frac{1}{2}\mu(v_\infty - u_{max})^2\right]$$

and

$$E_{max} = \frac{1}{2}\mu(v_\infty + u_{max})^2$$

In general, we believe it likely that in practical situations $v_\infty > u_{max}$, so that E is not zero within the sphere $\eta = 1$.

The number of collisions with energies between E and E + dE is the number which occurs in a shell bounded by the two ellipsoids at energies E and E + dE and the surface of the sphere $\eta = 1$. At any point on this surface, the shell thickness is

$$d\underset{\sim}{s} = dE/|\underset{\sim}{\nabla}E|$$

and the number of collisions associated with an elemental area dA of this surface is

$$\frac{d\dot{N}}{dA} = \dot{\nu}\, d\underset{\sim}{s} = \frac{d\dot{N}}{dV}\,\frac{dE}{|\nabla E|} \qquad (3.33)$$

The total number of collisions with the required energy then becomes the surface integral of $d\dot{N}/dA$ over the surface E = constant:

$$\frac{d\dot{N}}{dE} = \left| \int_{E=\text{const}} \frac{d\dot{N}}{dV}\,\frac{1}{|\nabla E|}\, dA \right| \qquad (3.34)$$

To evaluate this integral, it will prove easier to work in cylindrical coordinates. We introduce the variables $\underset{\sim}{r} = r/u_{max}t$ and $\underset{\sim}{z} = z/u_{max}t$ so that

$$E = \frac{1}{2}\mu\left[v_\infty^2 + u_{max}^2(\underset{\sim}{r}^2 + \underset{\sim}{z}^2) - 2v_\infty u_{max}\,\underset{\sim}{z}\right] \tag{3.35}$$

and

$$\frac{d\overset{\circ}{N}}{dV} = \underset{\sim}{n}_\infty \sigma D \frac{m\,u_{max}^3}{\bar{n}\,a_o^3}\left[1 - (\underset{\sim}{r}^2 + \underset{\sim}{z}^2)^{n/2}\right]^B \cdot$$

$$\left[v_\infty^2 + u_{max}^2(\underset{\sim}{r}^2 + \underset{\sim}{z}^2) - 2v_\infty u_{max}\,\underset{\sim}{z}\right]^{1/2} \tag{3.36}$$

The integral over the surface E = constant can be reduced to an integration in the plane z = 0 by projecting the surface on the plane. Thus if dA is the element of area on the surface E = constant and dA′ is the element of area in the plane z = 0, these elements are related as

$$dA = \left[\left(\frac{\partial \underset{\sim}{z}}{\partial \underset{\sim}{x}}\right)^2_{\underset{\sim}{y},E} + \left(\frac{\partial \underset{\sim}{z}}{\partial \underset{\sim}{y}}\right)^2_{\underset{\sim}{x},E} + 1\right]^{1/2} dA' \tag{3.37}$$

where $\underset{\sim}{x}^2 + \underset{\sim}{y}^2 = \underset{\sim}{r}^2$ and $dA' = d\underset{\sim}{x}\,d\underset{\sim}{y} = 2\pi \underset{\sim}{r}\,d\underset{\sim}{r}$. Since

$$\left(\frac{\partial \underset{\sim}{z}}{\partial \underset{\sim}{x}}\right)_{\underset{\sim}{y}E} = -\left(\frac{\partial E}{\partial \underset{\sim}{x}}\right)_{\underset{\sim}{y},\underset{\sim}{z}} \Big/ \left(\frac{\partial E}{\partial \underset{\sim}{z}}\right)_{\underset{\sim}{x},\underset{\sim}{y}}$$

and

$$\left(\frac{\partial \underset{\sim}{z}}{\partial \underset{\sim}{y}}\right)_{\underset{\sim}{x},E} = -\left(\frac{\partial E}{\partial \underset{\sim}{y}}\right)_{\underset{\sim}{x},\underset{\sim}{z}} \Big/ \left(\frac{\partial E}{\partial \underset{\sim}{z}}\right)_{\underset{\sim}{x},\underset{\sim}{y}} ,$$

we have

$$\left(\frac{\partial \underset{\sim}{z}}{\partial \underset{\sim}{x}}\right)_{\underset{\sim}{y},E} = \frac{\underset{\sim}{x}}{\underset{\sim}{z} - v_\infty/u_{max}}$$

and

$$\left(\frac{\partial \underset{\sim}{z}}{\partial \underset{\sim}{y}}\right)_{\underset{\sim}{x},E} = \frac{\underset{\sim}{y}}{\underset{\sim}{z} - v_\infty/u_{max}} \quad .$$

Then

$$dA = 2\pi \left[\frac{\underset{\sim}{r}^2}{(\underset{\sim}{z} - v_\infty/u_{max})^2} + 1\right]^{1/2} \underset{\sim}{r}\, d\underset{\sim}{r} \quad . \tag{3.38}$$

Also

$$\nabla E = \hat{\underset{\sim}{r}}\, \mu\, u_{max}^2\, \underset{\sim}{r} + \underset{\sim}{z}\, \mu\, (u_{max}^2\, \underset{\sim}{z} - v_\infty\, u_{max})$$

or

$$|\nabla E| = \mu\, u_{max}^2 \left[\underset{\sim}{r}^2 + (\underset{\sim}{z} - v_\infty/u_{max})^2\right]^{1/2} \tag{3.39}$$

so that

$$\frac{d\mathring{N}}{dE} = 2\pi \int_0^{\underset{\sim}{r}_{max}} \frac{d\mathring{N}}{d\overline{V}}\, \frac{\underset{\sim}{r}\, d\underset{\sim}{r}}{\mu\, u_{max}^2 (\underset{\sim}{z} - v_\infty/u_{max})^2} \quad . \tag{3.40}$$

The development is completed by eliminating the explicit $\underset{\sim}{z}$ dependence from Equation (3.40) and prescribing the limit of integration $\underset{\sim}{r}_{max}(E)$. First, we rewrite (3.35) as

$$(\underset{\sim}{z} - v_\infty/u_{max})^2 = \frac{2E}{\mu\, u_{max}^2} - \underset{\sim}{r}^2 \tag{3.41}$$

and (3.36) as

$$\frac{d\mathring{N}}{d\overline{V}} = \underset{\sim}{n}_\infty\, \sigma\, D\, \frac{m\, u_{max}^2}{\overline{n}\, a_o^3} \left[1 - \left(\frac{v_\infty^2}{u_{max}^2} - 2\, \frac{v_\infty}{u_{max}} \sqrt{\frac{2E}{\mu\, u_{max}} - \underset{\sim}{r}^2} + \frac{2E}{\mu\, u_{max}^2}\right)^n\right]^B \left[\frac{2E}{\mu}\right]^{1/2} \tag{3.42}$$

where the minus sign is chosen in the explicit expression for $\underset{\sim}{z}$ because of the requirement that $\underset{\sim}{z}^2 \leq 1 - \underset{\sim}{r}^2$ and the assumption that $v_\infty > u_{max}$. These expressions, when inserted into Equation (3.40), give an expression which depends only upon E and the other parameters of the calculation. Since if $v_\infty > u_{max}$ the tangent planes to the ellipsoids of constant E which lie parallel to the z-axis touch the ellipsoids at points outside the sphere $\eta = 1$, the value of r_{max} is determined by the intersection of the surface of constant E with the sphere $\eta = 1$:

$$\underset{\sim}{z}^2 = 1 - \underset{\sim}{r}^2_{max} = \frac{v_\infty^2}{u_{max}^2} - 2\frac{v_\infty}{u_{max}}\sqrt{\frac{2E}{\mu u_{max}^2} - \underset{\sim}{r}^2_{max}} + \frac{2E}{\mu u_{max}^2} - r^2_{max}$$

or

$$\underset{\sim}{r}_{max} = \left\{ \frac{2E}{\mu u_{max}^2} - \frac{1}{4}\frac{u_{max}^2}{v_\infty^2}\left[\frac{v_\infty^2}{u_{max}^2} + \frac{2E}{\mu u_{max}^2} - 1\right]^2 \right\}^{1/2} \qquad (3.43)$$

Again the minus sign is chosen to keep $\underset{\sim}{z}$ and $\underset{\sim}{r}$ less than 1.

For the general case, it appears necessary to solve Equation (3.18) by numerical methods, substitute the resulting values of $n_\infty(r,z,t)$ into Equation (3.36), and continue the subsequent integrations (with n_∞ under the integral sign) in order to arrive at a collision energy distribution. We have set this problem aside at the moment, and are currently checking out a small computer code which calculates the collision energy distributions in various situations. We also intend to perform a few spherically symmetric vacuum expansion calcu-

lations using the CELLS code (a one-dimensional, time-dependent Lagrangian flow code developed at Wayne State University) in order to examine Hubbard's choice of n under these conditions.

These calculations will give only a first approximation to the collision energy distribution at high altitude, since secondary collisions and the effects of ambient temperature have been omitted. Since including these effects requires a solution to the Boltzmann equation, by Monte Carlo or other procedures, we have no firm plans to include them. (The 1-D Monte Carlo code developed at Wayne State is suitable for the release geometry.) Since currently available information on the cross-sections of the most-important V-T excitation processes indicates that they have a strong dependence on collision energy, the first collision treatment appears to be a reasonable first approximation.

In the lower-altitude case, where continuum equations of motion are appropriate, we may compare particle histories as calculated by the CELLS and MULTITUBE codes. These comparisons will be forthcoming in the near future.

REFERENCES

1. F. P. Boynton, "Plume Observables and Countermeasures (Semi-Annual Technical Report No. 1, Contract F19628-72-C-0006)," Physical Dynamics Report PD-72-020, Feb., 1972.

2. J. P. Cahill, et al, "Airborne Infrared Plume Measurements of the Apollo 14 Boosters," Air Force Cambridge Research Laboratories, AFCRL-TR-71-0401, 28 June 1971.

3. W. Norman, M. Kinslow, and J.W.L. Lewis, "Experimental Study of Simulated High Altitude Rocket Exhaust Plumes," Von Karman Gas Dynamics Facility, Arnold Engineering Development Center, AEDC-TR-71-25, July 1971.

4. F. P. Boynton, E. R. Fisher, and J. Alex Thomson, "Rocket Exhaust Structure, Kinetics, and Radiative Properties at High Altitudes," Physical Dynamics Report PD-71- , January 1971.

5. F. P. Boynton, "High Altitude Rocket Plume Structure: Comparison of Experiment with Numerical Calculations," Physical Dynamics Report PD-72- , (in preparation).

6. E. R. Fisher, "Compilation and Review of Vibrational Excitation Cross-Section Calculations," Wayne State University, Research Institute for Engineering Sciences, (in preparation).

7. G. Moretti, "A New Technique for the Numerical Analysis of Non-Equilibrium Flows," AIAA J., 3, 223 (1965).

8. R. Marriott, "Calculation of Cross-Sections for Vibrational Excitation of Water, CO_2 and CO by Collision with Hydrogen and Water," General Dynamics/Astronautics Report GDA-DBE-64-059, Nov. 1964.

9. R. C. Millikan and D. R. White, "The Systematics of Vibrational Relaxation," J. Chem. Phys. 39, 3209 (1963).

10. I. Jamshidi, E. R. Fisher, and R. Kummler, "The Vibrational Temperature of N_2 in the E and F Regions," submitted to J. Geophys. Res.

11. J.C.G. Walker, Planetary Space Sci. 16, 33 (1968); J.C.G. Walker and R. Stolarski, Annal. Geophys. 25, 831 (1969).

12. E. R. Fisher, "The Chemistry of High Rocket Exhaust Plumes," Appendix I of IDA Study S-344, July 1969.

13. G. S. Bahn, "Evolution of a First-Round Reaction Kinetics Package for Pyrolysis/Combustion of a Large Aliphatic Hydrocarbon Molecule," Western States Section, The Combustion Institute, 1969 Fall Meeting, Menlo Park, Calif., Oct. 1968 (WSS/CI Paper 68-37).

14. E. R. Fisher and R. H. Kummler, private communication.

15. J. T. Herron and R. T. Huie, J. Phys. Chem. 73, 1326 (1969).

16. Ya. B. Zel'dovich and Yu. P. Raizer, Physics of Shock Waves and High-Temperature Hydrodynamic Phenomena, Vol. I, Academic Press, New York, 1966, pp. 93-106.

17. E. W. Hubbard, "Expansion of Initially Uniform Gas Clouds into Vacuum," AIAA J. 5, 378 (1967).

FIGURES

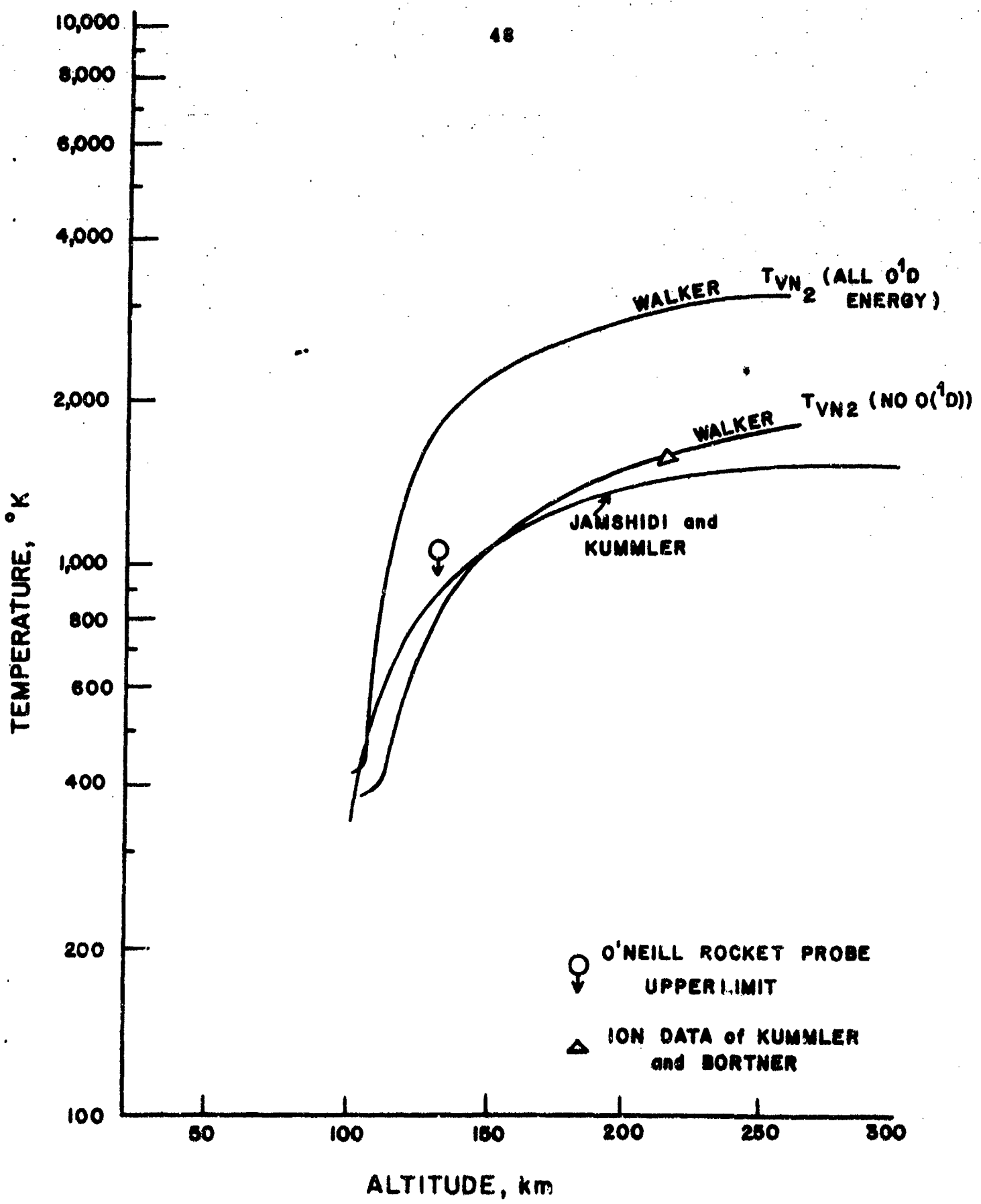

FIGURE 1. VIBRATIONAL TEMPERATURE OF N_2 AS A FUNCTION OF ALTITUDE IN THE IONOSPHERE

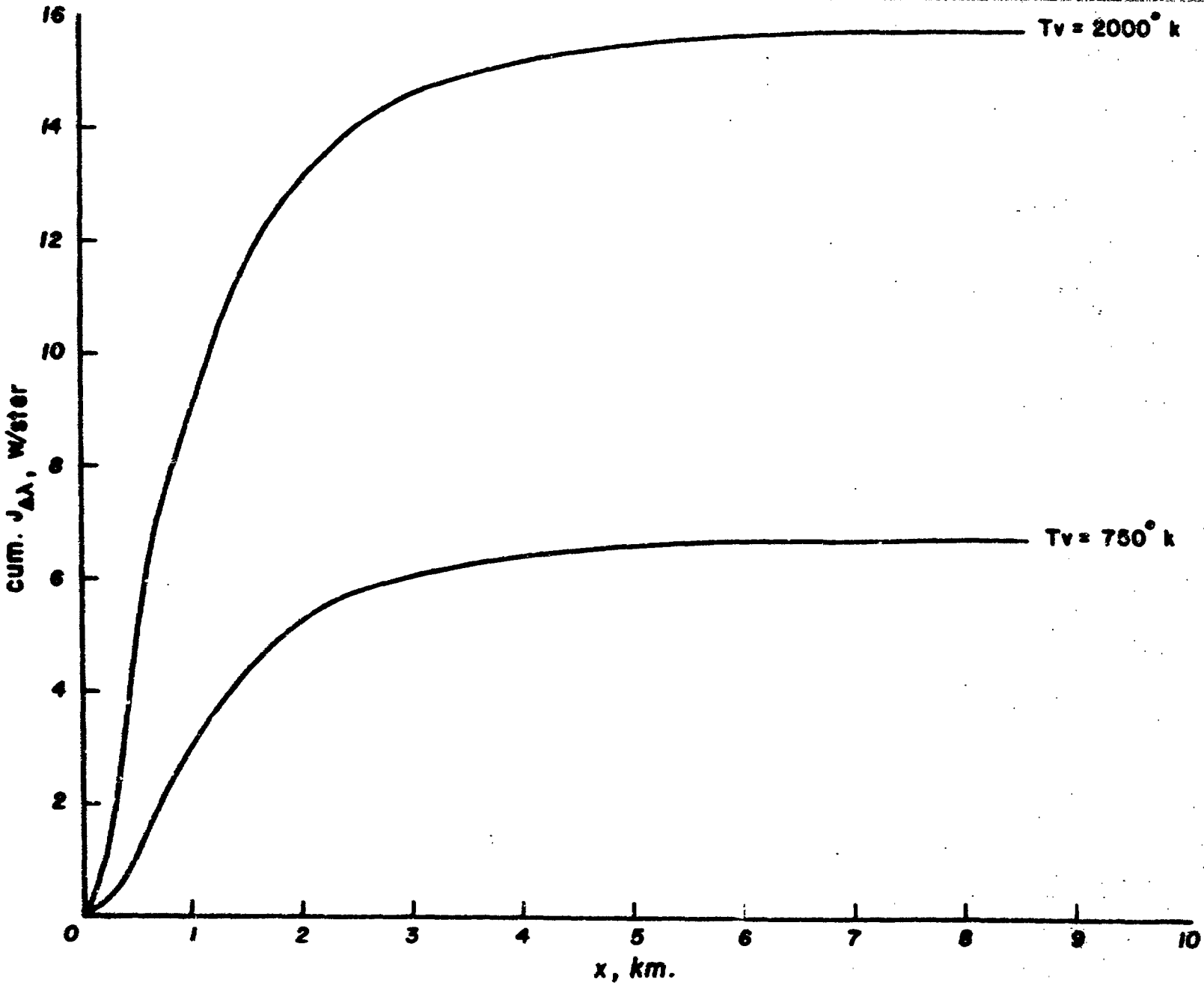

FIGURE 2. CUMULATIVE RADIANT INTENSITY OF THE "TURBULENT" APOLLO S-II PLUME AT 120 KM IN THE H_2O ν_1 OR ν_3 BANDS UPSTREAM OF A GIVEN AXIAL DISTANCE FOR TWO ASSUMED VALUES OF THE N_2 VIBRATIONAL TEMPERATURE ACCORDING TO THE "TWO-STEP" V-V,

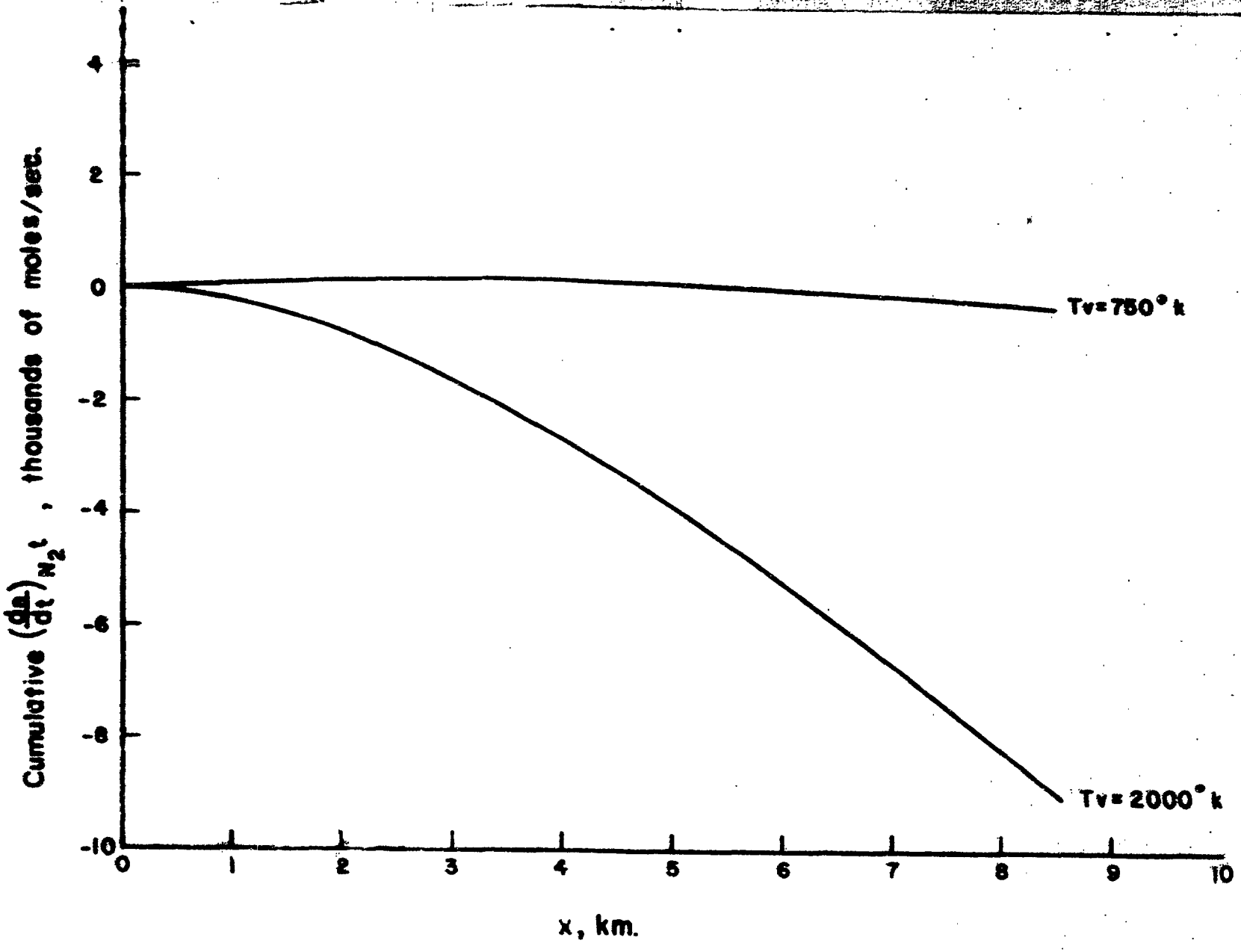

FIGURE 3. CUMULATIVE PRODUCTION OF VIBRATIONALLY-EXCITED N_2 IN THE "TURBULENT" APOLLO S-II PLUME AT 120 KM UPSTREAM OF A GIVEN AXIAL DISTANCE

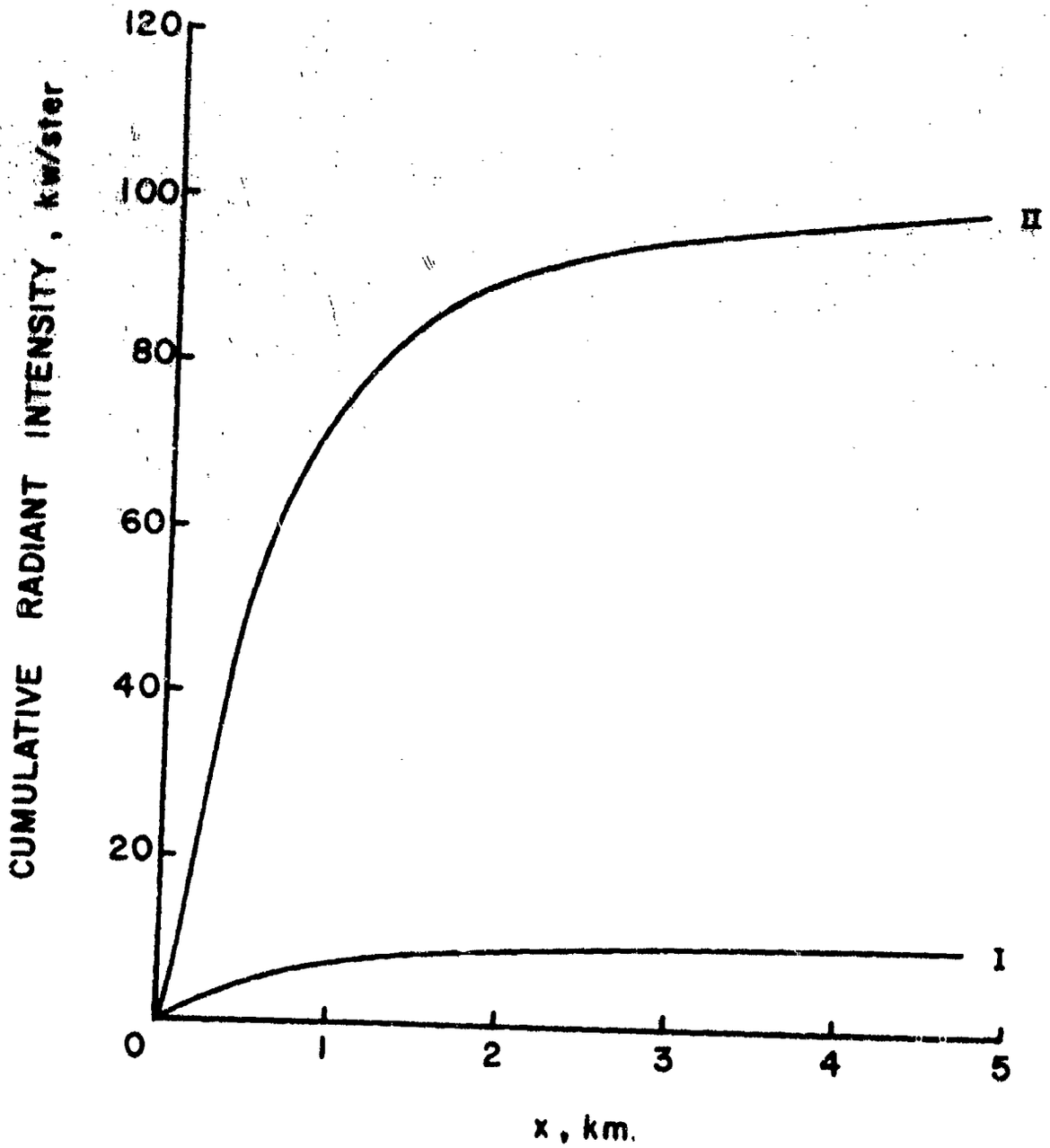

FIGURE 4. CUMULATIVE RADIANT INTENSITY OF THE LAMINAR ATLAS SUSTAINER PLUME AT 120 KM IN THE H_2O ν_1 OR ν_3 BANDS UPSTREAM OF A GIVEN AXIAL DISTANCE FOR THE OH CHEMILUMINESCENCE MECHANISM. FOR CURVE I, OH IS FORMED ONLY BY O + C_NH_{2N+2} ALSO CONTRIBUTES. TURBINE EXHAUST COMPOSITION BY MOLES IS 26% H_2, 11% CO, 4% CO_2, 1.3% H_2CO, 2.6% CH_4, 26% C_2H_6, 19.5% C_NH_{2N+2}.

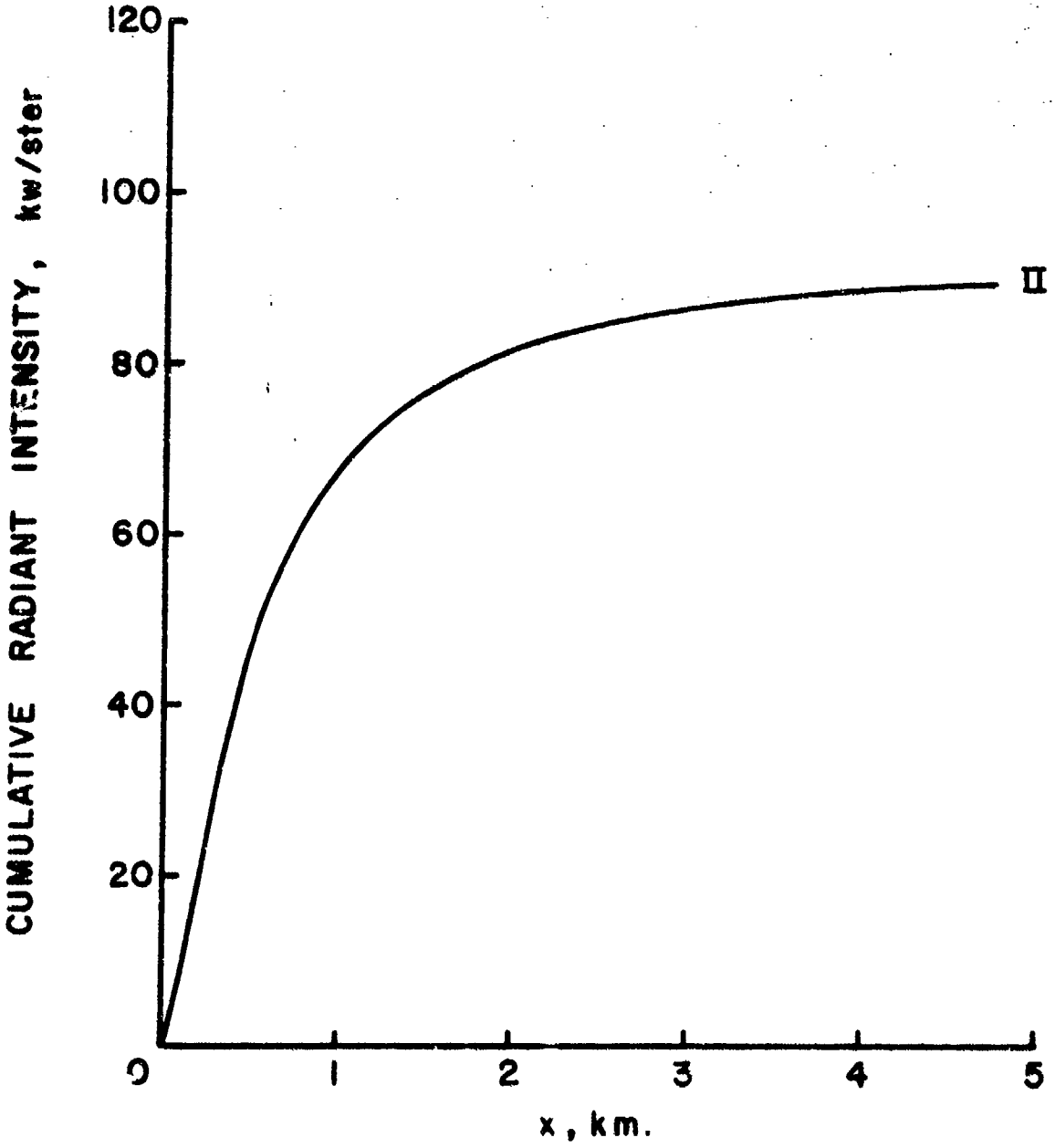

FIGURE 5. CUMULATIVE RADIANT INTENSITY OF THE LAMINAR ATLAS SUSTAINER PLUME AT 120 KM IN THE H_2O ν_1 OR ν_3 BANDS UPSTREAM OF A GIVEN AXIAL DISTANCE FOR THE OH CHEMILUMINESCENCE MECHANISM. CONDITIONS AS IN FIGURE 4 EXCEPT THAT CH_2O MOLE FRACTION IS 0.65%, C_NH_{2N+2} MOLE FRACTION IS 20.2%.

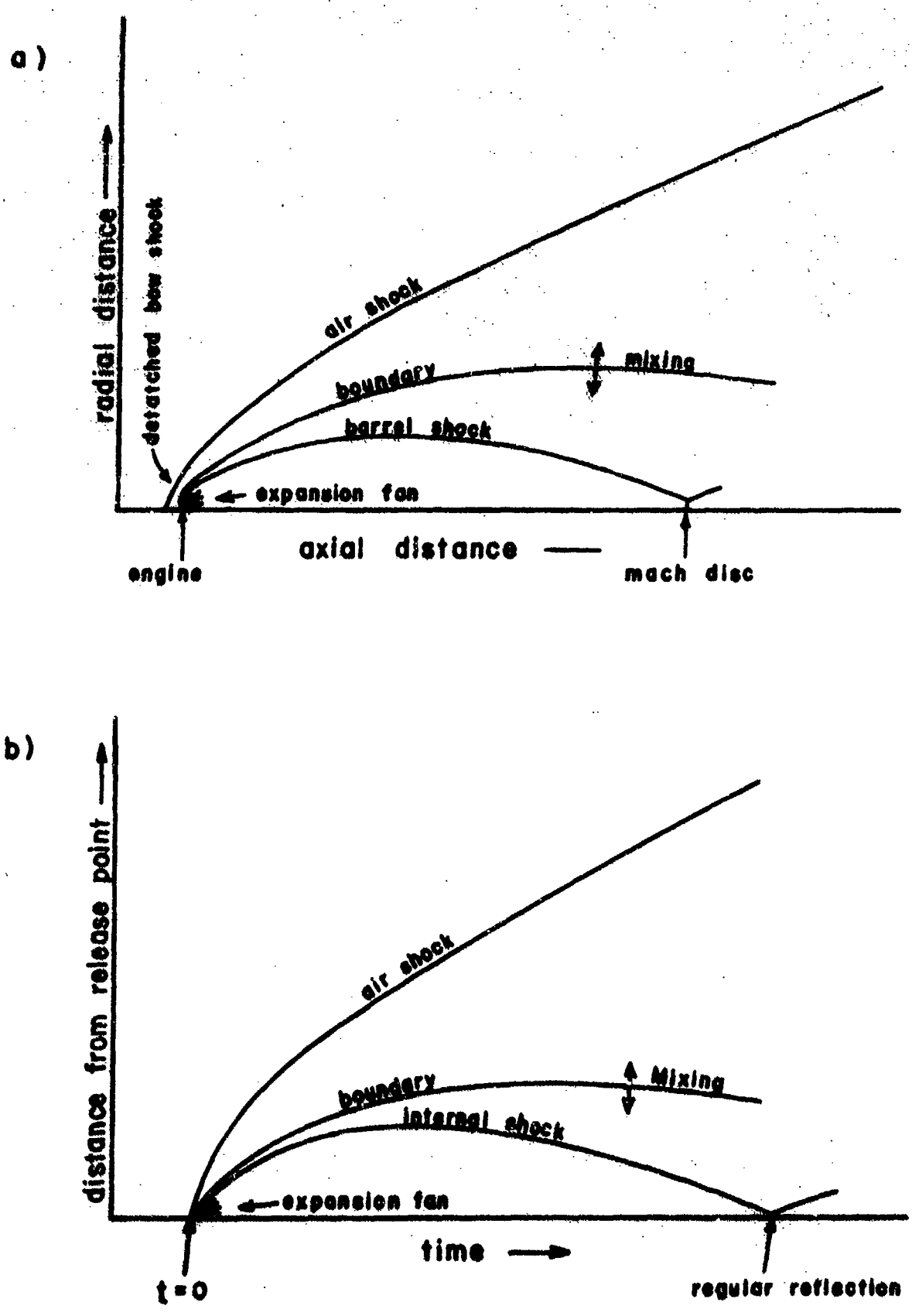

FIGURE 6. GENERAL STRUCTURE OF ROCKET EXHAUST PLUMES (A) AND MATERIAL RELEASES (B) IN THE UPPER ATMOSPHERE AT LOW AMBIENT PRESSURES. CONTINUUM HYDRODYNAMICS ASSUMED.

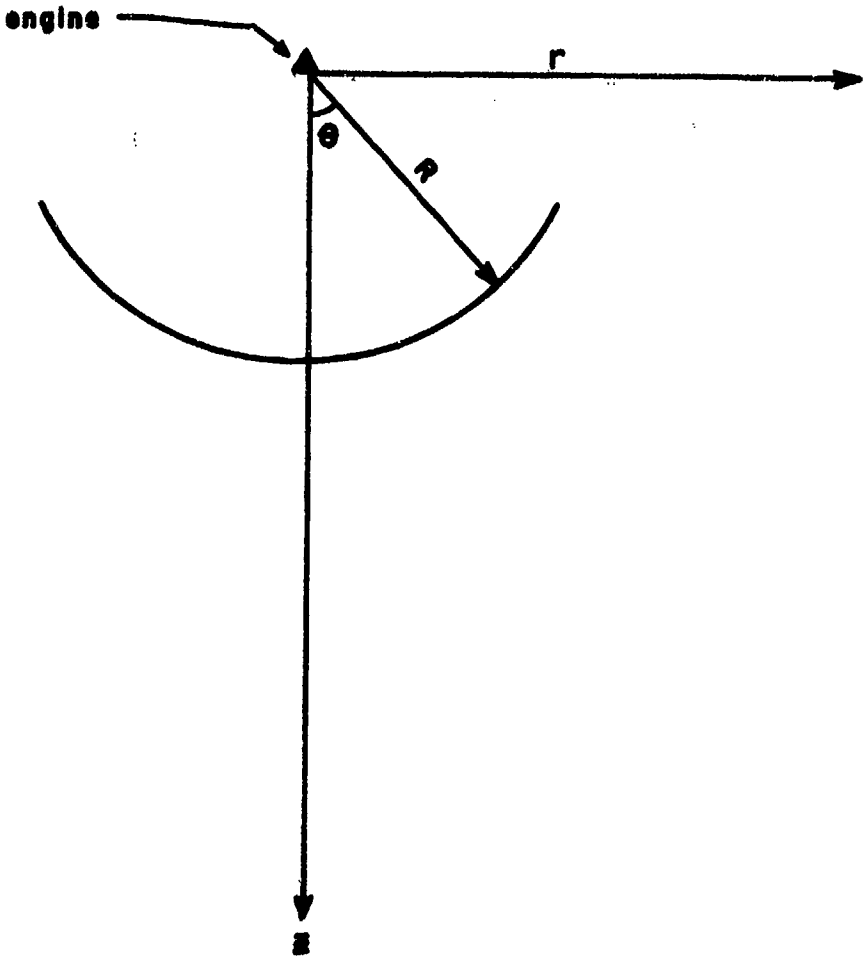

FIGURE 7. COORDINATE SYSTEM FOR DESCRIBING ROCKET EXHAUST PLUME FLOW AND INTERACTIONS WITH THE FREE STREAM

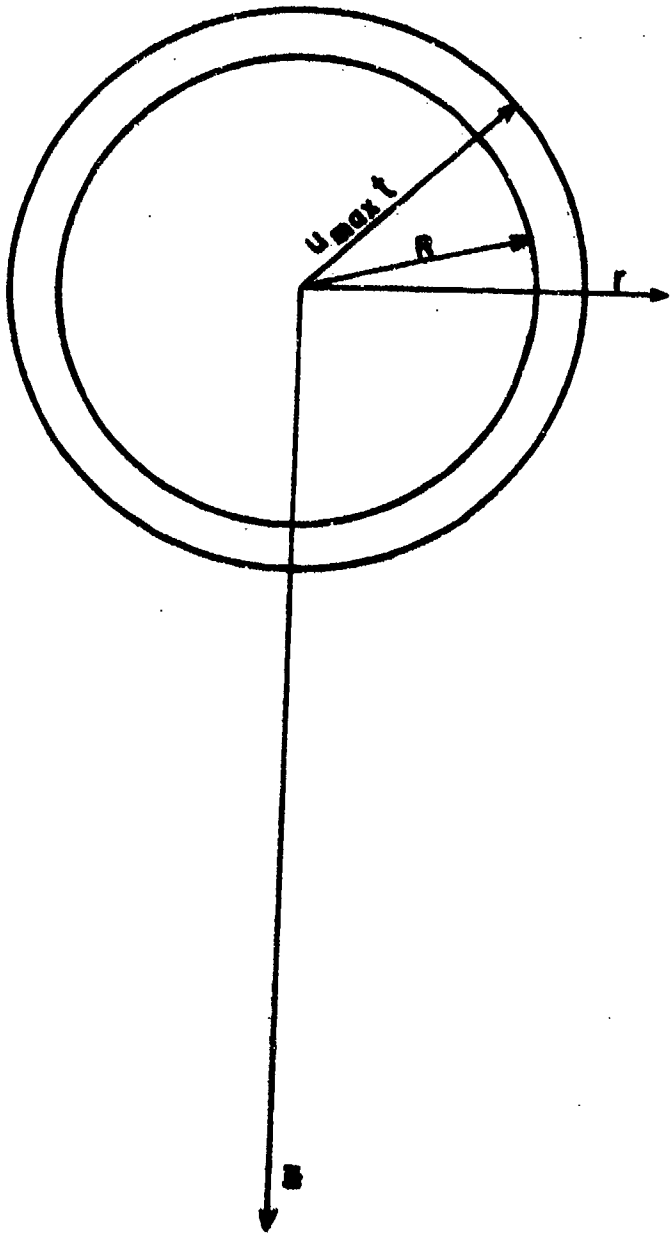

FIGURE 8. COORDINATE SYSTEM FOR DESCRIBING SPHERICAL RELEASES AND THEIR INTERACTIONS WITH AMBIENT GAS

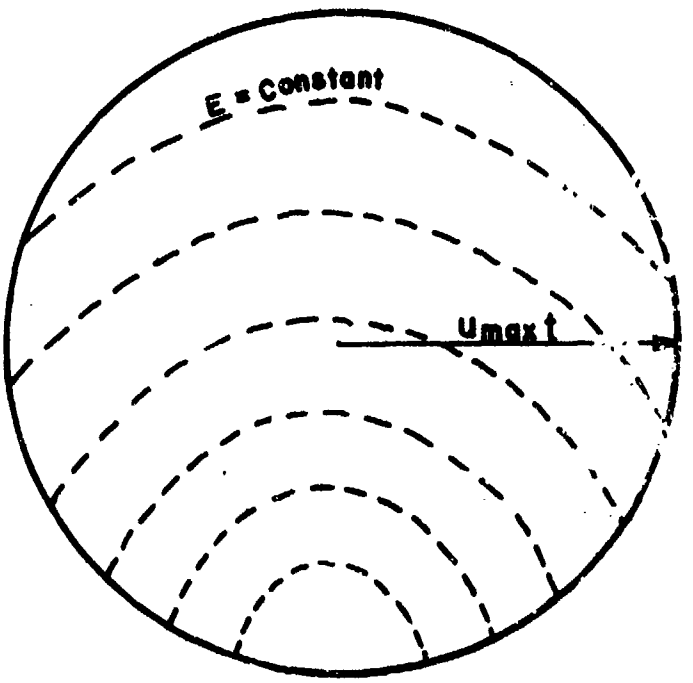

FIGURE 9. SURFACES OF CONSTANT FIRST COLLISION ENERGY BETWEEN ATMOSPHERIC MOLECULES AND RELEASED GASES WHEN THE INITIAL VELOCITY OF THE RELEASED MATERIAL IS LARGE